

Argentinean Copper Concentrates: Structural Aspects and Thermal Behaviour

Vanesa Bazan^{1*}, Elena Brandaleze², Leandro Santini², Pedro Sarquis³

¹CONICET—Instituto de Investigaciones Mineras, Universidad Nacional de San Juan, San Juan, Argentina

²Metallurgical Department and Technology and Materials Develop Center, DEYTEMA-Universidad Tecnológica Nacional, Facultad Regional de San Nicolás, Colón, Argentina

³Instituto de Investigaciones Mineras, Universidad Nacional de San Juan, San Juan, Argentina
Email: *bazan@unsj.edu.ar, ebrandaleze@frsn.utn.edu.ar, psarquis@unsj.edu.ar

Received July 4, 2013; revised August 5, 2013; accepted August 28, 2013

Copyright © 2013 Vanesa Bazan *et al.* This is an open access article distributed under the Creative Commons Attribution License, which permits unrestricted use, distribution, and reproduction in any medium, provided the original work is properly cited.

ABSTRACT

In Argentina, there are many sources of copper concentrates. Some of them are currently in operation, while others are in the exploration stage. All copper concentrates produced are exported to other countries for copper refinement and to create various finished products. It is desirable that in the near future, these copper concentrates be processed in an Argentinean industrial plant. The aim of this paper was to present the results of a characterisation study carried out on five different copper concentrate samples. The thermal decomposition of the copper concentrates was determined by differential thermal analysis and thermogravimetry (DTA TG). The information was correlated with the chemical composition and the mineralogical phases of the samples identified by X-ray diffraction. A melting test at temperatures of up to 1300°C was performed to complete the study of the concentrate's behaviour during heating. After the test, all of the samples were observed by light and electronic scanning microscopy to identify the different phases generated under high-temperature conditions.

Keywords: Copper Concentrates; Thermal Analysis; Pyrometallurgy; Mineral Phases

1. Introduction

The copper market is undoubtedly one of the most important metallic markets in the world. This statement is based on the significantly increased global demand for this metal and its alloys in recent years.

Argentina has large reserves of copper ores and constitutes a strong supplier of concentrates in our region [1-4]. The ores selected for this study contain between 0.5% - 0.8% copper and are free of impurities such as Sb, As, Te and Se. Currently, concentrates obtained by flotation operations are exported to other countries to produce final copper products such as wires, pipes and sheets [5]. It is important to promote the installation of a copper pyrometallurgy plant in our country to allow for the ability to process concentrates and create final products for Argentina's domestic market. Copper industrial processes include melting, conversion and refining operations [6]. To design the pyrometallurgy process, it is necessary to completely characterise the concentrates. Thus, it is necessary to obtain information about the current phases

that exist in concentrate particles and the type of transformations and reactions that occur under processing conditions [7].

Winkel *et al.* [8] described the importance of enhancing the knowledge about the high-temperature behaviour of copper iron sulphides, as well as the volatile impurities they contain. This information is essential to develop new processes of extractive metallurgy.

Thermal analysis techniques, such as differential thermal analysis (DTA) and thermogravimetry (TG), represent important tools to determine the concentrates' behaviour during the decomposition of copper iron sulphides and sulphur volatilisation rates [8-12].

In this paper, information regarding the thermal behaviour of five samples of Argentinean copper concentrates is presented. The results obtained by DTA and TG were correlated with information determined by X-ray diffraction (XRD) and a microscopy study. Structural analyses of the concentrate samples were performed after the melting tests. The test products were examined by electron microscopy (SEM), and the phases were identified by XRD. The authors describe the mechanisms, such

*Corresponding author.

as mass transport, which allow for the separation of metallic copper.

2. Materials and Methods

2.1. Samples

Five samples of copper concentrates obtained by Rougher flotation were selected for this study. The copper ores were obtained from sources located in northern Argentina.

2.2. Methods

The concentrate characterisation was carried out. The chemical composition of each sample was determined by acid attack and atomic absorption spectrometry using a Perkin Elmer AA110 instrument. The crystal phases were identified by X-ray diffraction (XRD) at room temperature using a Philips X'Pert diffractometer. The sulphide quantification was conducted by applying the ASTM standard C25 [13].

A microscopy study performed using an Olympus GX51 light microscope and applying a LECO IA32 analysis system, which allowed for the observation of the types of particles and their morphological characteristics.

Another objective of this paper was to evaluate the behaviour of the concentrates at high temperatures. To obtain information about the reactions that occur during heating, melting tests were carried out at temperatures of up to 1300°C in air. Samples were melted in a porcelain

crucible using an electric furnace. All of the melted samples were prepared for microscopy observation. Their structure was studied using light and scanning electron microscopy (SEM). Finally, the results were correlated with the DTA-TG results.

3. Results

3.1. Chemical Composition

The chemical composition of the five concentrates samples is presented in **Table 1**.

3.2. Mineral Phases

The X-ray diffraction results provide information regarding the crystalline phases present in the five samples studied. The major minerals present in the concentrates were chalcopyrite (CuFeS_2), pyrite (Cu_2S) and iron sulphide (FeS). Nevertheless, other minerals such as iron bisulphide (FeS_2), geerite (Cu_8S_5), enargite (Cu_3AsS_4) and dicopper zinc silicon tetrasulphide ($\text{Cu}_2\text{Zn SiS}_4$), among others, were identified. However, sample E was observed to contain a lower chalcopyrite content and higher pyrite content. In sample B, geerite (Cu_8S_5), enargite (Cu_3AsS_4) and dicopper zinc silicon tetrasulphide ($\text{Cu}_2\text{Zn SiS}_4$) were identified, and in sample C, PbS was identified. Traces of cassiterite (SnO_2) were identified in samples A and D. **Figures 1-5** show the diffractograms of all of the samples, specifically the principal peaks corresponding to the crystal phases observed.

Table 1. Chemical composition of the copper concentrates samples.

(a)

Sample	Cu%	Fe%	Ins%	SiO ₂ %	R ₂ O ₃ %	CaO%	MgO%	S%	Al ₂ O ₃ %
A	16.9	32.1	2.76	1.64	53.12	0.15	0.08	37.6	8.78
B	22.3	31.4	1.70	0.88	51.58	0.18	0.08	35.2	8.25
C	18.4	31.5	1.64	1.04	52.96	0.14	0.05	37.8	9.43
D	14.6	33.1	2.52	1.28	55.06	0.11	0.07	38.9	9.35
E	18.1	35.3	2.04	0.52	59.36	0.13	0.05	33.3	10.59

(b)

Sample	Sb ppm	As ppm	Se ppm	Te ppm
A	<50	52	<50	<30
B	<50	68	<50	<30
C	<50	48	<50	<30
D	<50	35	<50	<30
E	<50	49	<50	<30

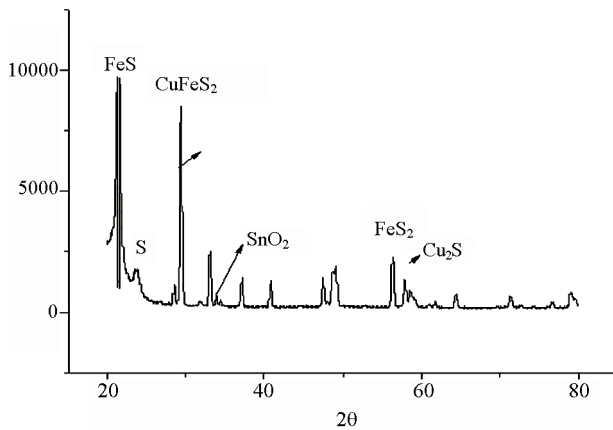


Figure 1. Sample A diffractogram.

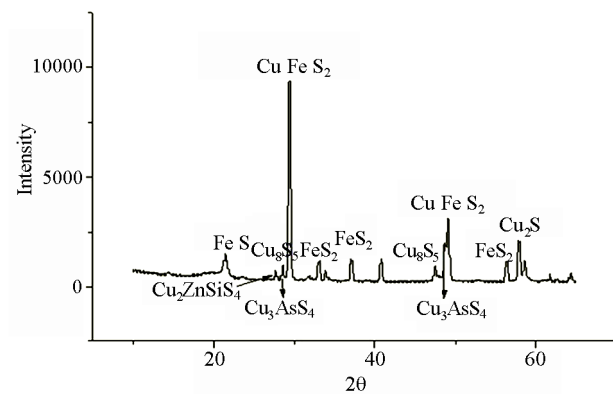


Figure 2. Sample B diffractogram.

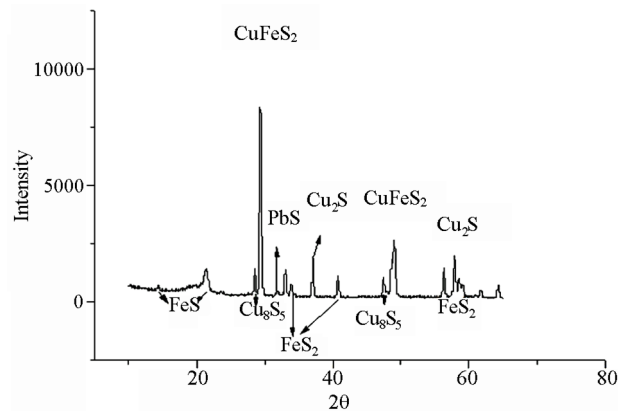


Figure 3. Sample C diffractogram.

3.3. Thermal Analysis Tests

DTA and TG tests were carried out at a heating rate of 10°C/s using a JENCK instrument. In this manner, the mechanisms of oxidation during heating up to 1000°C were characterised for all of the copper concentrate samples. For each sample, the first exothermic peak temperature, T_{in} , was determined. This temperature establishes the beginning of the oxidation reaction. The

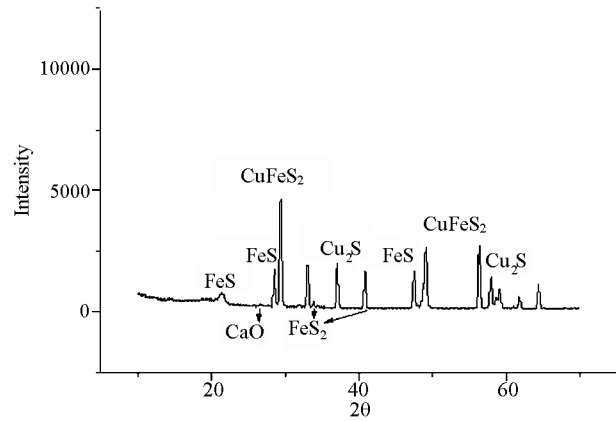


Figure 4. Sample D diffractogram.

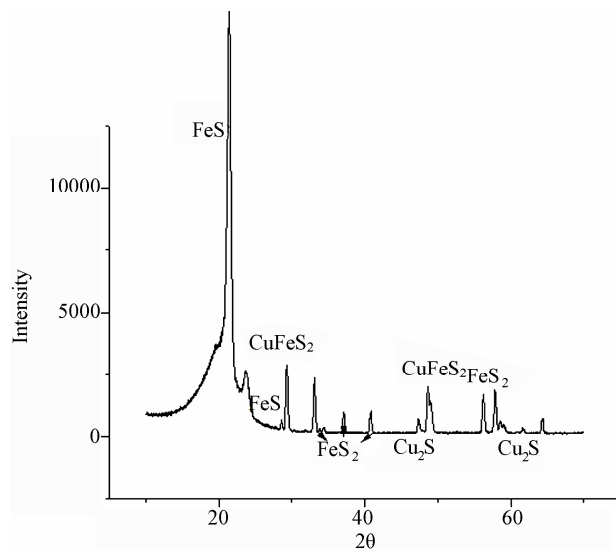


Figure 5. Sample E diffractogram.

exothermic heat, Q_{ex} , was determined by the area below the DTA curve. These values represent the total heat that developed during all of the reactions. Both values are very useful for understanding the flash-melting process [11,12,14,15].

Figure 6 shows the DTA curves of the five samples. The T_{in} and Q_{ex} values calculated by numerical integration are presented in Table 2. Notably, both values are related to the oxygen content of the copper, which in this case, are constant.

The thermogravimetric curves (TG) (Figure 7) allow for the observation of mass changes and losses in the concentrate samples during heating.

3.4. Melting Test

Samples of each copper concentrate were melted in porcelain crucibles at 1200°C at a heating rate of 5°C/min in air. The structure of the solidified product of each sample was studied by light and scanning electron microscopy

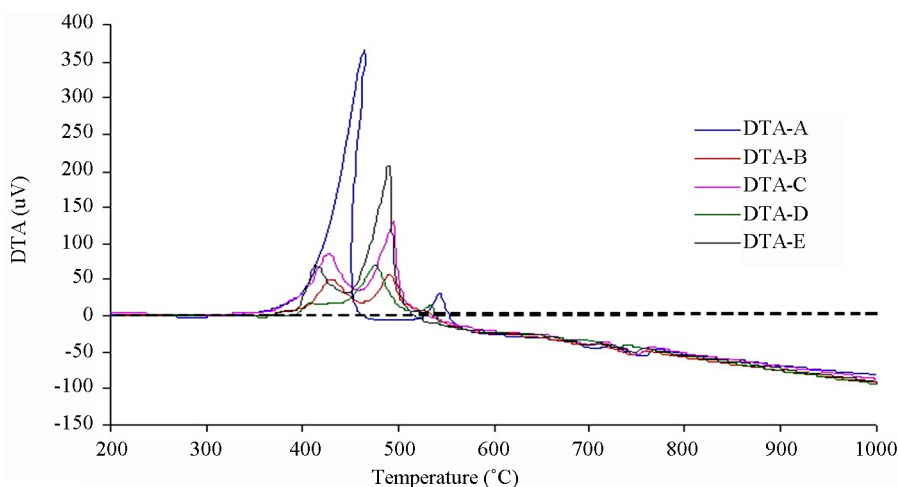


Figure 6. DTA curves of the five copper concentrates samples.

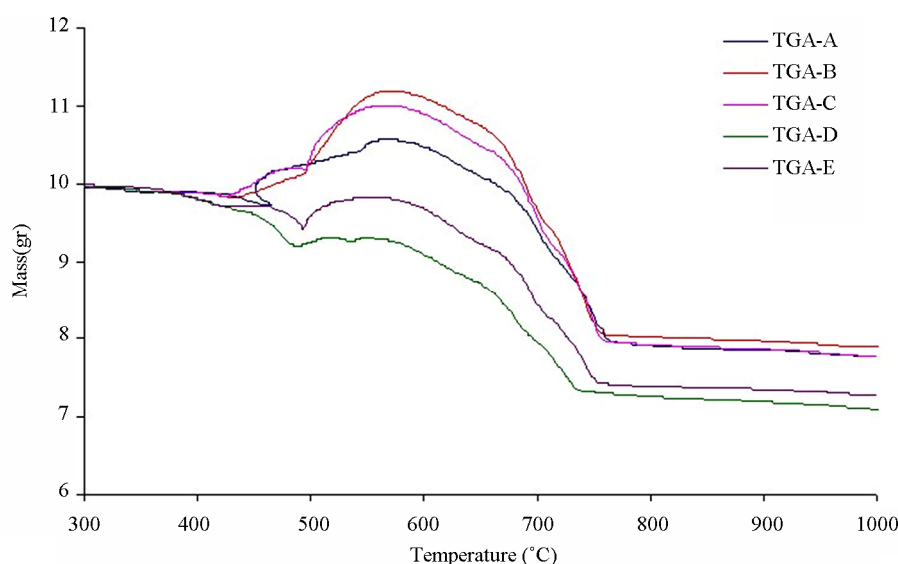


Figure 7. Thermogravimetric curves of the copper concentrates.

Table 2. Values of the initial oxidation temperature T_{in} , exothermic heat Q_{ex} and the copper law of the concentrates.

Sample	Copper law (%)	T_{in} (°C)	Q_{ex} (KJ/Kg)
A	16.86	309 ± 10	13880 ± 300
B	22.28	344	5185
C	18.38	340	7328
D	14.65	390	3254
E	18.03	415	12225

(SEM). In all cases, three different layers were recognised: a greyish layer with a fine dispersion of white particles (located in the bottom of the crucible), a white (intermediate) layer that contained a large number of dendritic crystals and extensive porosity and finally a top grey layer composed of spherical and irregular white

particles of a larger size with respect to the bottom-layer particles. **Figure 8** shows a vertical cross section of the solidified layers in sample A.

Notably, in the intermediate white layer, native copper bands (**Figure 9**) and white dendrites were observed. A higher proportion of native copper bands and globular particles was observed in sample B. In the grey top layer, white crystals with different morphologies, irregular, needle-shaped and dendritic, were observed.

In samples B, C, D and E, the bottom and top grey layers were observed to be thicker than those in sample A and to contain a low proportion of white particles. However, in all of the samples, the intermediate white layer was observed to contain metallic copper bands.

The phases were examined by SEM in the three layers. Elemental mapping revealed the elemental distribution in each layer. **Table 3** shows the elemental distribution ob-

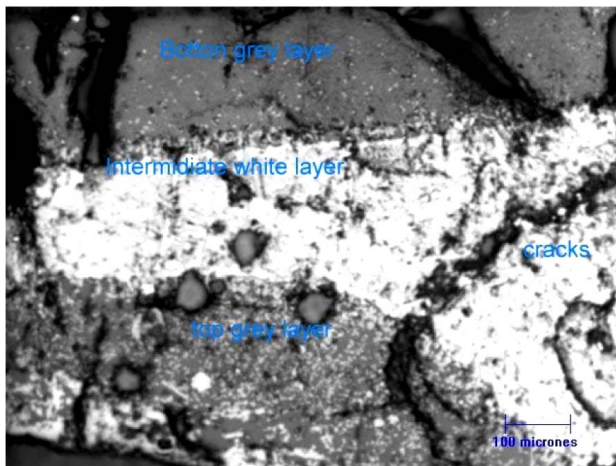


Figure 8. Three layers present in the structure of solidified product A.

served in sample A.

The bottom grey layer of the samples contains white particles of silicoaluminate. A few particles of CuS and phases with higher iron contents were observed near the interface in contact with the intermediate white layer. Also, traces of other elements such as Mg and Cr in the silicoaluminate matrix were detected.

The intermediate white layer contains metallic copper bands, white dendrites or irregular crystals of (Cu, Fe)S, and the matrix has a high iron sulphide (FeS) content.

The white and the grey top layers were observed to be porous. Sample D showed the highest porosity among the samples studied.

The top grey layer matrix consists of calcium silicoaluminate and copper sulphide particles (with dendritic and globular morphologies). Traces of K, Ti and Cr were identified. Irregular copper particles isolated in the layer and in the microcracks were also observed.

If we consider copper, iron and sulphur to be the main elements and approximate their content to be 100%, it is possible to plot on a ternary diagram the sulphide composition identified in the intermediate white layer and in the grey top layer. For simplicity, the plotted compositions correspond to samples A and D (**Figure 10**).

These two samples were selected because of the phases differences observed. Samples B, C and E contain phases similar to those observed in sample A but in different proportions. Notably, the sulphide phases developed under the test conditions (1200°C) show copper contents up to 52%.

4. Discussion

The chemical composition of the concentrates show that sample B possessed a higher Cu content (22.28%) and a lower content of Fe (31.40%). Importantly, sample B also exhibited the lowest S/Cu ratio (1, 58).

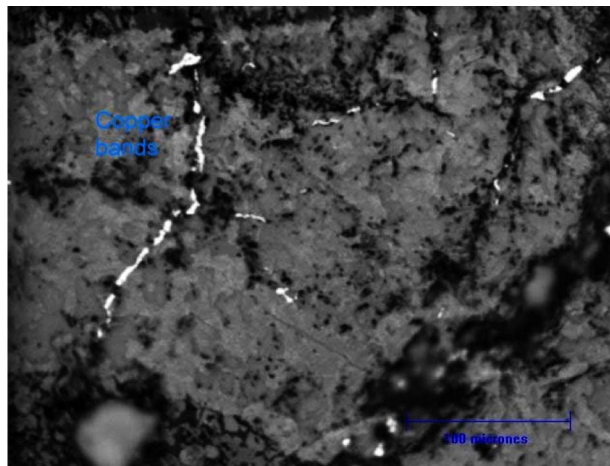


Figure 9. Copper band observed in the intermediate.

Sample D contained the lowest concentration of Cu (14.65%) and the highest S and Fe concentrations. Moreover, the S/Cu ratio of sample D was 2.65, which is highest value observed in the concentrate samples. The XRD results are consistent with the chemical composition results.

Based on the DTA results, the correlation between the T_{in} and Q_{ex} values with respect to the law of copper concentration (Cu(X)) can be modelled by third-degree polynomial equations, (Equations (1) and (2)) for which $R = 0.9946$.

$$T_{in} (^{\circ}C) = 1.425(X)^3 - 78.488(X)^2 + 1377.8(X) - 7490.8 \quad (1)$$

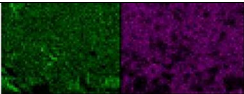
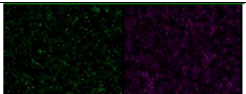
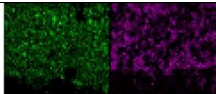
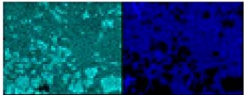
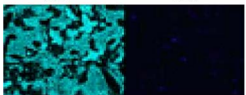
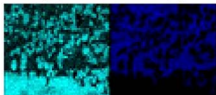
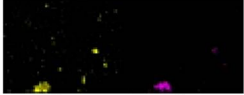
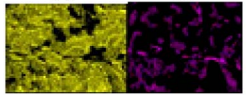

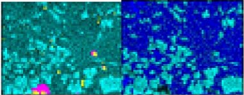
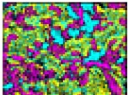
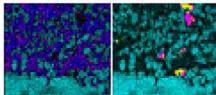
$$Q_{ex} (KJ/Kg) = -215.6(X)^3 + 14335(X)^2 - 268157(X) + 2 \cdot E^{+6} \quad (2)$$

The T_{in} values vary with mineralogical composition and respect the following order of the samples: $A < C < B < D < E$. As observed experimentally, sample B has an intermediate initial oxidation temperature. A higher content of pyrite indicates an increase in T_{in} because of the high melting temperature of the compound. Nevertheless, the other phases in the concentrates also affect T_{in} .

The exothermic heat Q_{ex} values were obtained by the numerical integration of the exothermic peaks on the DTA curves (**Figure 6**). The exothermic heat is generally associated with the oxygen content present during the test. However, in this case, the oxygen concentration is constant. Thus, it is possible that the higher value is due to the chalcopyrite (CuFeS₂) and coveline (CuS) contents.

The DTA and TG curves show that the sample-B reactions develop with low Q_{ex} , which is associated with a significant loss of mass during heating between room temperature and 1000°C. A gradual weight loss in the

Table 3. Element distribution in the three layers of the post melted sample A.

Bottom grey layer	Intermediate white layer	Top grey layer
		
		
		
		

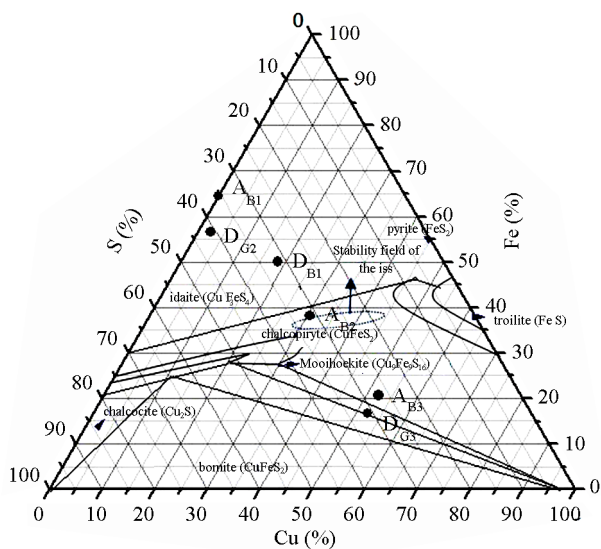


Figure 10. Sulphide composition determined in the white (B) intermediate layer and in the grey (G) top layer of samples A and D.

range of 300°C to 450°C was observed for all of the concentrates. This change is attributed to humidity loss. In particular, sample E exhibited a drastic loss of mass at 500°C; this is because the range 450°C - 550°C favours the direct oxidation of pyrite to loadstone, while at temperatures above 650°C the complete elimination of any formed ferrous sulphate is favoured; this is manifested as weight loss [16].

A gradual increase in mass up to 600°C was observed for all of the concentrate samples. The transformation of the sulphides into oxides coincides with these mass-change exothermic peaks (in DTA curves). A new and pronounced loss of mass up to 750°C was observed for the five concentrates. At these temperatures, the trans-

formations are probably associated with the sulphide and SO₂ dissociation.

The proposed reaction mechanisms, based on the behaviour indicated by the DTA and TG curves and the equilibrium information obtained by calculation using the software program HSC (Outokumpu), are detailed in **Table 4**.

The DTA results are consistent with proposed reaction 5, which implies a loss of mass because of the sulphide-to-oxide transformation. In addition, it is important to consider the chalcopyrite (CuFeS₂) transformation (reactions 3 and 4).

The initial mass loss revealed by TG is based on the decomposition of a pure Cu₂S sample and the oxidation of pyrite, as observed in reactions 5 and 6.

The gradual increase in mass determined by the TG test at 600°C was also reported by Perez-Tello *et al.* [17]. They believed that the concentrates quickly gain mass through the copper sulphate formation. However, **Figure 11** shows that reactions 11 and 10 contribute to the increase in mass through the formation of iron sulphide. Although this species is later dissociated, as indicated by reaction 14, the reaction speed is slow due to that the formation of sulphates, which closes the pores of the particle and prevents the reaction from occurring, and thus creates a gain in mass, as shown in **Figure 7** [16].

The gradual final loss of mass is explained by the decomposition reactions of the sulphate into oxides.

Samples B and C showed the same behaviour during heating because of their similar mineralogical composition: high content of chalcopyrite (CuFeS₂) and low copper and iron sulphides in the concentrate. These samples developed intermediate T_{in} and Q_{ex} during heating.

Sample A presented a lower T_{in} and higher Q_{ex} because of the higher contents of chalcopyrite (CuFeS₂)

Table 4. Reaction mechanisms.

Reaction	$-\Delta G^\circ$ (kcal) _{reacc}	Mass changes %	Reaction number
$5\text{CuFeS}_2 + 9\text{O}_2(\text{g}) = \text{Cu}_3\text{FeS}_4 + 2\text{Fe}_2\text{O}_3 + 6\text{SO}_2(\text{g})$	653 – 621	-10.50	1
$2\text{Cu}_3\text{FeS}_4 + 14.5\text{O}_2(\text{g}) = 10\text{CuO} + \text{Fe}_2\text{O}_3 + 8\text{SO}_2(\text{g})$	876 – 788	-4.85	2
$2\text{CuFeS}_2 + 6.5\text{O}_2(\text{g}) = 2\text{CuO} + \text{Fe}_2\text{O}_3 + 4\text{SO}_2(\text{g})$	436 – 406	-8.59	3
$2\text{CuFeS}_2 + 6\text{O}_2(\text{g}) = \text{Cu}_2\text{O} + \text{Fe}_2\text{O}_3 + 4\text{SO}_2(\text{g})$	410 – 387	-17.50	4
$2\text{FeS}_2 + 5.5\text{O}_2(\text{g}) = \text{Fe}_2\text{O}_3 + 4\text{SO}_2(\text{g})$	388 – 377	-33.44	5
$2\text{FeS} + 3.5\text{O}_2(\text{g}) = \text{Fe}_2\text{O}_3 + 2\text{SO}_2(\text{g})$	273 – 253	-9.17	6
$\text{Cu}_2\text{S} + 2\text{O}_2(\text{g}) = 2\text{CuO} + \text{SO}_2(\text{g})$	113 – 98	-0.04	7
$\text{Cu}_2\text{S} + 1.5\text{O}_2(\text{g}) = \text{Cu}_2\text{O} + \text{SO}_2(\text{g})$	86 – 79	-10.09	8
$2\text{Cu}_3\text{FeS}_4 + 2\text{SO}_2(\text{g}) + 19.5\text{O}_2(\text{g}) = 10\text{CuSO}_4 + \text{Fe}_2\text{O}_3$	1066 – 781	74.91	9
$2\text{CuFeS}_2 + 9\text{O}_2(\text{g}) + \text{SO}_2(\text{g}) = 2\text{CuSO}_4 + \text{Fe}_2(\text{SO}_4)_3$	532 – 403	95.92	10
$\text{FeS}_2 + 3\text{O}_2(\text{g}) = \text{FeSO}_4 + \text{SO}_2(\text{g})$	203 – 176	233.33	11
$\text{Cu}_2\text{S} + 2.5\text{O}_2(\text{g}) = \text{CuO} * \text{CuSO}_4$	125 – 90.61	50.26	12
$2\text{Cu}_2\text{O} + \text{O}_2(\text{g}) = 4\text{CuO}$	14 – 5	11.17	13
$2\text{FeSO}_4 + 1.5\text{O}_2(\text{g}) = \text{Fe}_2\text{O}_3 + 2\text{SO}_2(\text{g}) + 2\text{O}_2(\text{g})$	6 – 26	-47.44	14
$\text{Fe}_2(\text{SO}_4)_3 = \text{Fe}_2\text{O}_3 + 3\text{SO}_2(\text{g}) + 1.5\text{O}_2(\text{g})$	3 – 41	-60.06	15
$2\text{CuSO}_4 + \text{O}_2(\text{g}) = 2\text{CuO} + 2\text{SO}_2(\text{g}) + 2\text{O}_2(\text{g})$	+10 – 14	-50.16	16
$2\text{CuO} * \text{CuSO}_4 = 4\text{CuO} + 2\text{SO}_2(\text{g}) + \text{O}_2(\text{g})$	+13 – 10	-33.48	17

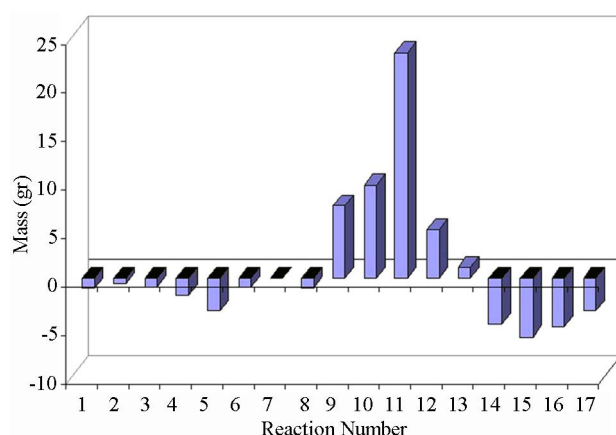


Figure 11. Mass evolution with respect to reaction mechanisms.

and iron sulphide (FeS), promoting an intermediate change in weight.

Sample E, which contained the highest percentage of FeS, showed a combination of higher Q_{ex} and T_{in} . The mass lost by this sample is lower than that by samples A, B and C.

The microscopy study of the five concentrates solidified samples showed that the contents of chalcopyrite and iron sulphide (*i.e.*, sample A) in the concentrates increase with the thickness of the white layer. In all samples, this white intermediate layer featured native copper bands or globular particles because of the decomposition of sulphides. In this case, the (Cu, Fe)S exhibited 31%

Cu.

In the top grey layer matrix, white dendrites or irregular crystals of (Cu, Fe)S in a matrix with a higher iron sulphide (FeS) content were identified. These phases were observed in the greatest quantity in samples D and E. (Cu, Fe)S contained approximately 52% Cu.

Based on the S-Cu-Fe system, it was possible to conclude that different sulphide phases formed at the selected melting test conditions (1200°C, 1 h) in both layers (A_B or D_B in the white intermediate layer and A_G or D_G of the grey top layer) contain up to 52% copper. Chalcopyrite decomposes at 623 K to an intermediate solid solution (ISS) (see Figure 10) or to chalcopyrite with a slightly different composition ($\text{CuFeS}_{2\text{ssb}}$); moreover, an iron sulphide transformation occurred. The presence of native copper in all of the samples indicates that sulphur was only partly removed.

5. Conclusions

To summarise, the characterisation of the five concentrates studied in this work revealed that these materials contained about 14% to 22% copper and that sample B was the richest in copper. The major copper minerals were sulphides: chalcopyrite (CuFeS_2) and coveline (CuS). Iron was present in the concentrates in the form of FeS_2 or FeS. Samples A and E showed the highest iron sulphide contents

The thermal analysis techniques applied in this study provided information that allowed us to determine the

initial oxidation temperature T_{in} and the exothermic heat Q_{ex} of the samples, as well as the mass changes during heating to 1000°C.

By correlating the DTA and TG results with the crystal phases identified by XRD and the information obtained through the thermodynamic equilibrium study performed using the software program HSC (Outokumpu), it was possible to identify the complex reaction mechanisms involved during concentrate heating. The reaction evolution features an initial transformation of the sulphides to oxides; then, the oxides react to form sulphates and are finally transformed to oxides. These results were confirmed by the phases identified by microscopy and the thermodynamic study on the Cu-Fe-S system.

REFERENCES

- [1] "Peralta e. Actas de Encuentro Internacional de Minería," Secretaría de Minería de la Nación. Buenos Aires, Argentina, 1994, pp. 5-15.
- [2] Segemar, Servicio Geológico Minero de Argentina. http://www.segemar.gov.ar/P_Oferta_Regiones/Oferta/Introducción.htm
- [3] A. Beretta and V. Bazan, "Algunos Fundamentos de las Ventajas Estratégicas de la Instalación de una Fundición de Cobre en Argentina," SAM/CONAMET, San Nicolás, Buenos Aires, 2007, pp. 7-12.
- [4] A. Guitierrez, D. Chong and R Espinoza, "Niveles de Exposición de Yacimientos del Distrito Minero de agua de Dionisio (YMAD)," *Revista de la Asociación Geológica Argentina, Catamarca*, Vol. 61, No. 2, 2006, pp. 269-277.
- [5] V Bazan, P Sarquis and E. Brandaleze, "Caracterización de un Mineral de Cobre en Argentina para la Producción de Matte," *Revista Dyna*, No. 167, 2011, pp. 220-228.
- [6] V. Bazán, P. Sarquis and E. Brandaleze, "Factibilidad de una Industria Pirometalurgia con Mineral Argentino Iras," *Jornadas de Investigación de la Minería del norte Argentino Editorial Científica Universitaria, Universidad Nacional de Catamarca*, 2009.
- [7] J. Dunn and C. Muzenda, "Thermal oxidation of covellite (CuS)," *Thermochimica Acta*, Vol. 369, No. 1-2, 2001, pp. 117-123. [http://dx.doi.org/10.1016/S0040-6031\(00\)00748-6](http://dx.doi.org/10.1016/S0040-6031(00)00748-6)
- [8] L. Winkel, I. Alxneit and M. Sturzenegger, "Thermal Decomposition of Copper Concentrates under Concentrated Radiation-Mechanistic Aspects of the Separation of Copper from Iron Sulfide Phases," *International Journal of Mineral Processing*, Vol. 88, No. 1-2, 2008, pp. 24-30. [http://dx.doi.org/10.1016/S0040-6031\(00\)00748-6](http://dx.doi.org/10.1016/S0040-6031(00)00748-6)
- [9] H. Tsukada, Z. Asaki, T. Tanabe and Y. Kondo, "Oxidation of Mixed Copper-Iron Sulfide," *Metallurgical Transactions B-Process Metallurgy*, Vol. 12, No. 3, 1981, pp. 603-609. <http://dx.doi.org/10.1007/BF02654333>
- [10] M. Perez-Tello, H. Y. Sohn and J. Lottiger, "Determination of the Oxidation Characteristics of Solid Copper Matte Particles by Differential Scanning Calorimetry and Thermogravimetric Analysis," *Minerals & Metallurgical Processing*, Vol. 16, No. 2, 1999, pp. 1-7.
- [11] J. Dunn and S. Jayaweera, "Applications of Thermoanalytical Methods to Studies of Flash Smelting Reactions," *Thermochimica Acta*, Vol. 85, 1985, pp. 115-118. [http://dx.doi.org/10.1016/0040-6031\(85\)85543-X](http://dx.doi.org/10.1016/0040-6031(85)85543-X)
- [12] Z. Zivkovic, N. Strbac, D. Zivkovic, V. Velinovski and I. Mihajlovic, "Kinetic Study and Mechanism of Chalcocite and Covellite Oxidation Process," *Journal of Thermal Analysis and Calorimetry*, Vol. 79, No. 3, 2005, pp. 715-720. <http://dx.doi.org/10.1007/s10973-005-0601-1>
- [13] ASTM C25-99, "Stándar Test Methods for Chemical Analysis of Limestone, Quicklime and Hydrated Lime," 1999.
- [14] F. Jorgensen and P. Koh, "Combustion in Flash Smelting Furnaces," *JOM*, Vol. 53, No. 5, 2001, pp. 16-21. <http://dx.doi.org/10.1007/s11837-001-0201-x>
- [15] S. Perez-Fontes, "Determinación de las Características de Oxidación de Minerales Sulfurosos a Altas Temperaturas," Tesis de Licenciatura en Ingeniería Química, Universidad de Sonora, Hermosillo Sonora, 2004.
- [16] V. Arias, R. Coronado, L. Puente and D. Lovera, "Refractariedad de Concentrados Auríferos," *Revista del Instituto de Investigación de la Facultad de Ingeniería Geológica, Minera, Metalúrgica y Geográfica*, Vol. 8, No. 16, 2005, pp. 5-14.
- [17] S. Perez-Fontes, M. Perez-Tello, L. Prieto, F. Brown and F. Castillon-Barraza, "Thermoanalytical Study on the Oxidation of Sulfide Minerals at High Temperatures," *Minerals & Metallurgical Processing*, Vol. 24, No. 4, 2007, pp. 275-283.